1.14 The MIT Model of the ACIS CCD

We have developed a detailed model of the frontside illuminated CCD response to the X-ray illumination. The model is based on the Monte-Carlo technique. Photons of given energy are thrown into the random positions on the CCD surface and the device reaction is calculated for each individual photon. The most important new features of our model are discussed below.

1.14.0.1 Absorption in the gate structure

X-ray photon can be absorbed in any material with an exponentially distributed (depthwise) probability of interaction. To model this process the simulation program generates an exponentially distributed random number R. If $R > \frac{d}{\lambda}$ we assume that the photon have passed the layer of thicknness d with characteristic absorption length λ without being absorbed. Otherwise the photon is absorbed inside the layer.

The cross section of the gate structure of the ACIS CCD along the direction of charge transfer is shown schematically on Fig. 1.124. Another cross-section, perpendicular to the

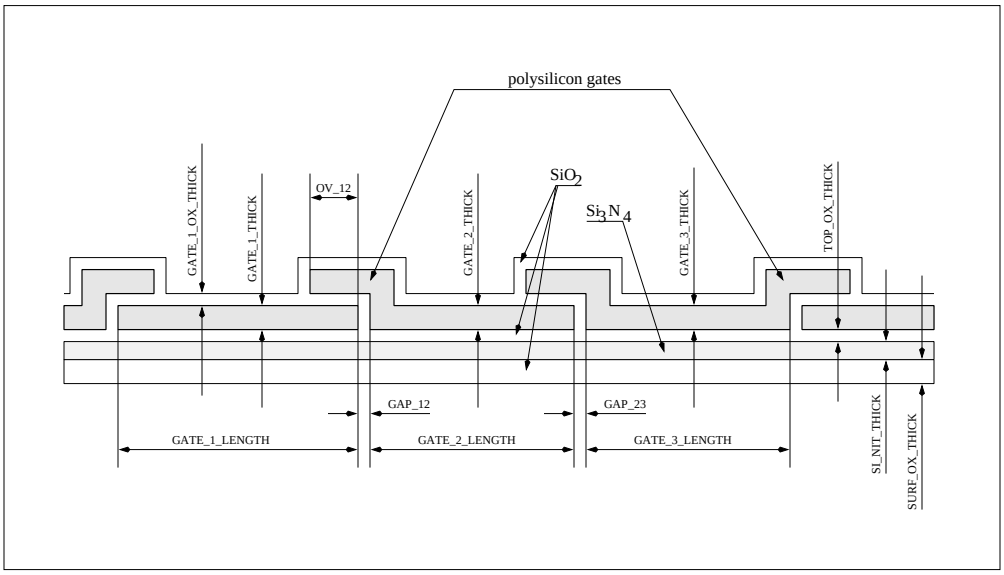

Figure 1.124: Cross section of the gate structure of the CCD along the transfer channel.

direction of the charge transfer is shown on Fig. 1.125. Electron microscope photographs clarifying the real life details of both cross-sections are shown on the Figures 1.43 and 1.44.

Absorption of X-rays in the gates becomes a very significant factor at low energies (below 1 keV) and immediately above silicon edge. Our model simulates all the details of

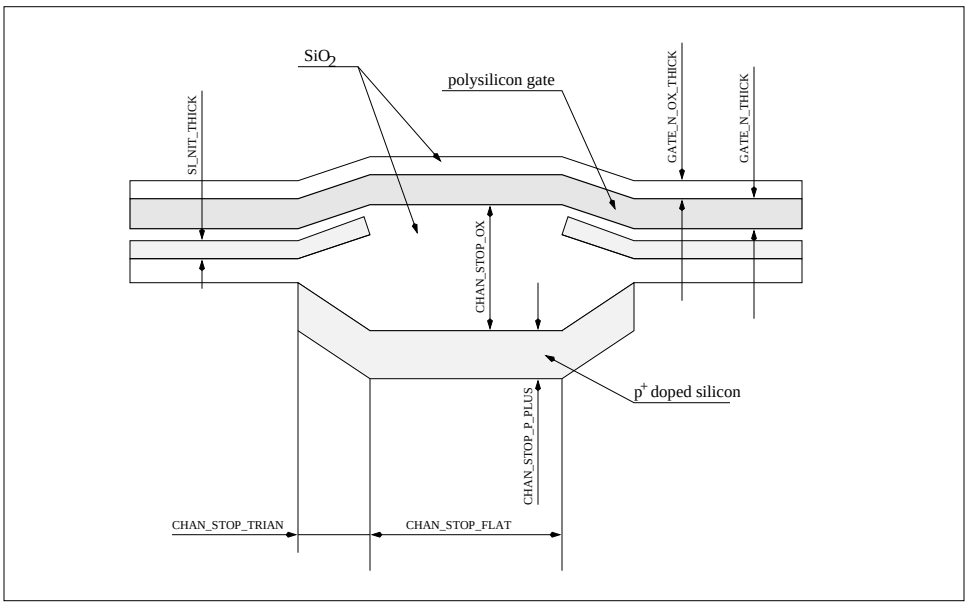

Figure 1.125: Cross section of the gate structure of the CCD perpendicular to the transfer channel.

the gate structure such as gate overlaps, oxide walls at the edges of the polysilicon gates, triangular shape of the wings of the oxide layer above the channel stop regions.

Characteristic absorption lengths for all the constituent layers are calculated based on the high precision measurements of the thin films of the corresponding materials performed at synchrotron beamlines (see subsection 1.6.4). As a result the model can very accurately predict quantum efficiency of the device in the entire energy range. It has a capability to show the distribution of the intensity of the detected fluxs across the pixel, which can be important for the subpixel resolution studies (see Chapter 6). Figures 1.126 and 1.127 demonstrate variations in sensitivity inside the pixel at the energies immediately below and above oxygen absorption edge for a pixel cross-section along the transfer channel.

Slightly different gate thicknesses (the values were obtained in the mesh experiment, see section 1.5) result in different intensity under different gates. Sharp drops in the sensitivity can be seen in the regions where adjacent gates overlap. Silicon dioxide is less opaque than silicon below oxygen absorption edge and more opaque immediately above the edge. Because of this jumps in sensitivity corresponding to oxidized edges of the gates inside overlap regions go in opposite directions at the two energies.

1.14.0.2 Fluorescence events

Simulating CCD response we assume that for each photon with energy greater than the silicon absorption K edge (1839 eV) absorbed inside silicon, there is a 0.043 probability to emit a fluorescent photon with the characteristic energy of 1.739 keV. We neglect the fluorescence from other elements (oxygen and nitrogen) as well as L-shell fluorescence of silicon due to a very small probabilities of these events. The fluorescent photons are emitted uniformly in all directions and the program calclulates the spatial angles using random number generator. After that the absorption probability for the fluorescent photons is calculated in the same manner as for a regular photon. If the fluorescent photon leaves silicon substrate or interacts several pixels away from the site of interaction of the primary photon, an escape event will be detected. The model makes an accurate prediction of the escape peak amplitude.

An amplitude of the fluorescent peak was much harder to reproduce. The key to the correct model of the flourescent peak, especially at energies close to the Si absorption edge, is taking into account fluorescence from the gates. Immediately above Si edge absorption in the polysilicon gates becomes a significant factor. Of the absorbed photons 4.3% produce a fluorescent photon and roughly half of them goes into the bulk of silicon and gets detected, while another half is emitted into the upper hemisphere and is lost. Unlike flourescent photons that are emitted from the bulk silicon, the leftover charge corresponding to the difference in energy between primary and fluorescent photon cannot be detected when it is formed in the polysilicon gate. This means that approximately half of the photons fluoresced from the gates will be found in the fluorescent peak, while only a tiny fraction of the ones from the bulk will end up in the fluorescent peak. Because of this flourescence from the gates is by far a dominant factor in forming the flourescence peak. On Fig. 1.128 are shown the amplitudes of the escape and flourescence peaks both from experimental data and simulated eventlists. The experimental data had been collected at a synchrotron ring at BESSY using Crystal Monochromator Beamline with a device w102c3.

Solid lines on Fig. 1.128 show the model predictions. An agreement between the data and the model is good. A discrepancy in the amplitudes of the fluorescence peak reported previously in the Preliminary Calibration Report is now resolved. It was caused mostly by not taking into account fluorescence from the gate structure.

1.14.0.3 Formation and diffusion of an electron cloud

When the photon interacts with a silicon atom in a detector an electron cloud is formed. If the interaction occured in the depleted layer, the electrons are pulled by an electric field and the cloud drifts into CCD potential wells spreading wider due to diffusion process at the same time. If the cloud was formed in the undepleted bulk of silicon, the electrons spread

out without drifting component, the ones that reach the border with the depleted region are carried by the electric field into the potential wells of the CCD. The final cloud size is an important parameter which determines how the charge of the cloud is split between adjacent pixels. We use the most common approach and calculate the final cloud radius r according to the formula $r = \sqrt{r_i^2 + r_d^2}$, where r_i is initial cloud radius, r_d - cloud radius due to diffusion process. To calculate the diffusion radius for charge generated both in depleted and undepleted bulk we follow the paper of Hopkinson [20]. For the initial cloud radius we use the results of Scholze&Ulm [21] if the interaction of the photon with the silicon atom did not occur near the $Si - SiO_2$ interface. Events which origin within a small distance from the surface lose some charge to the oxide layer and form a low energy tail of the response function. The treatment of such events is described in the subsection 1.3.2, the original cloud radius for them being much smaller than for the bulk events.

Also, different procedure is used for the charge clouds that are formed in the doped area of channel stops. We have shown (see [22]) that events originating in the p^+ region of the channel stop suffer a charge loss and as a result form a shoulder at the low energy side of the main peak. Since the majority of the events in the channel stops is split between two adjecent pixels, this effect is most pronounced for the horisontally split events. A histogram of the horizontally split events (ASCA grades 3 and 4) at 1487 eV is shown in Fig. 1.129. We have measured a fraction of the events in the shoulder relative to the total number of counts in the horizontally split histogram as a function of energy. The corresponding plot is shown on Fig. 1.130. It indicates that all the lossy events in the channel stop area come from a shallow region about 0.3 microns deep.

To take this phenomenon into account in our model for all charge clouds having their centers inside this region we introduce a loss which is a function of to the cloud charge and the cloud center location. As a result our model can reproduce low energy tail of the horizontally split events reasonably well.

1.14.0.4 Splitting of charge between pixels and writing to an output file.

Once the cloud sizes and cloud centers are known, the final calculations are fairly common for this kind of model. The cloud is split between adjacent pixels assuming gaussian distribution of charge density in the cloud. This implies a very simple routine for evaluating of the signal amplitude in pixels adjecent to the cloud center. After that a readout noise with gaussian distribution is added to each pixel and the gain factor is introduced to adjust the amplitude of the signal to that of the paticular device that is being modeled. The last stage is an event finding routine - a procedure similar to the one used in data analysis software to determine whether the amplitude of event is big enough to be written down into an eventlist. The output of the program is a standard eventlist which is entirely

compatible with numerous software tools available for the real data analysis. In Figures 1.131 and 1.132 are shown standard grade histograms for the experimental data taken under monochromatic illumination at 4510 eV and the simulated histograms for the same energy. While there are some small discrepancies, all the important features of the response, such as escape and fluorescent peaks, low energy peak, low energy tail, peculiar shape of the low energy tail of the horizontaly split events, are reflected in the model, and the agreement between the model and the data in general is good.

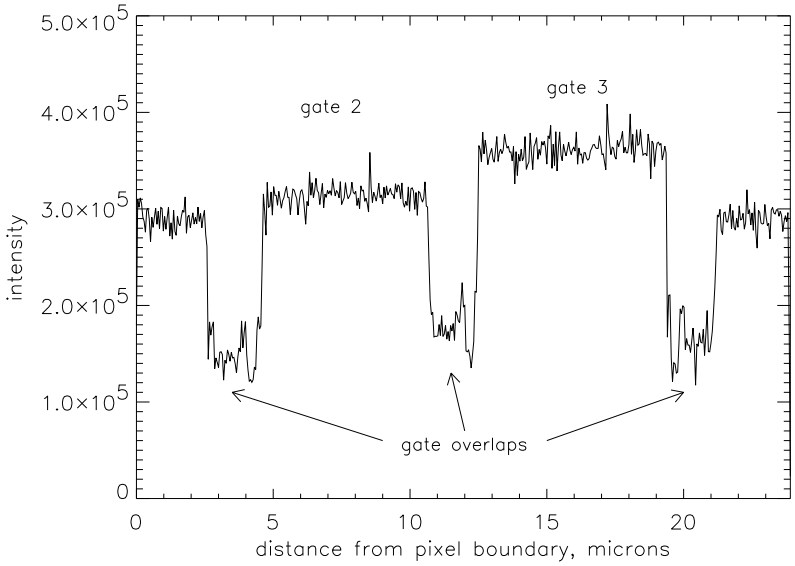

Figure 1.126: Number of detected events as a function of coordinate inside a single pixel. Energy of the incident photons is 525 eV.

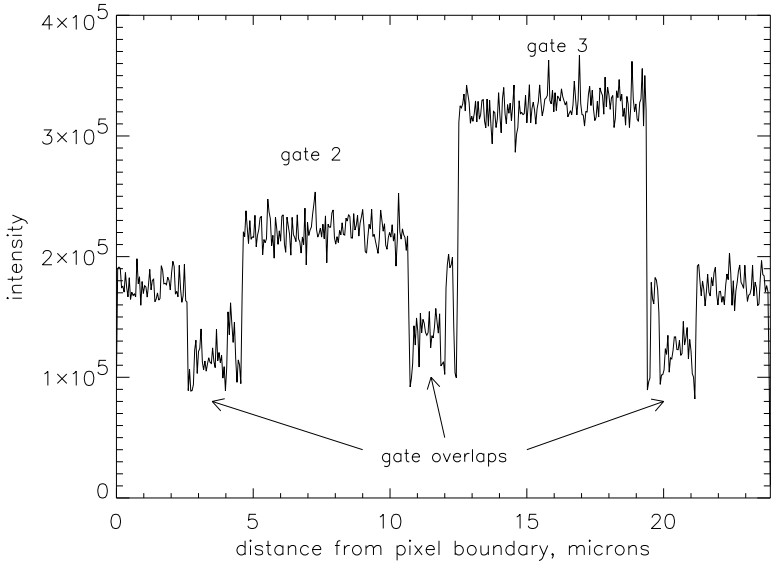

Figure 1.127: Number of detected events as a function of coordinate inside a single pixel. Energy of the incident photons is 539 eV, right above oxygen K edge. Notice a different behavior inside overlap regions

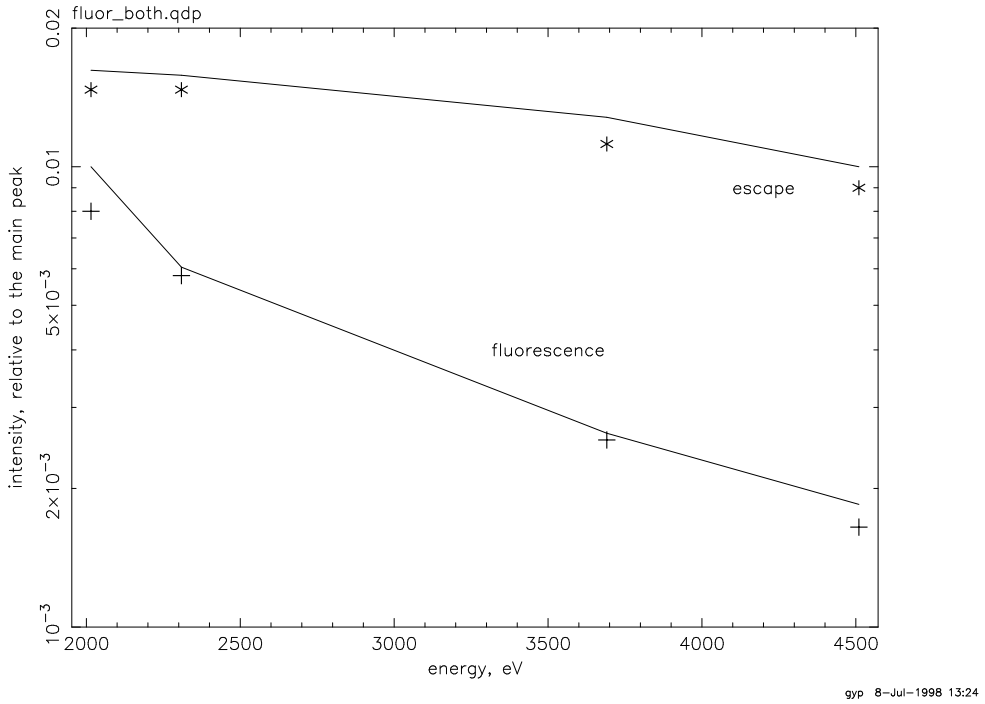

Figure 1.128: Intensities of experimentally measured escape (*) and fluorescence (+) features as a function of energy. Solid lines are the model predictions.

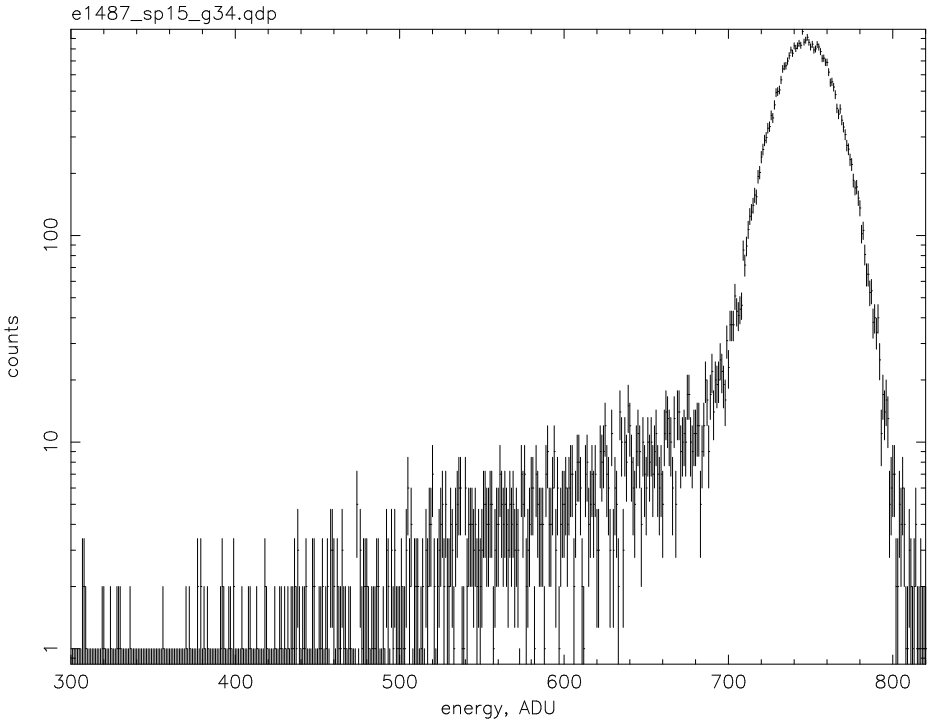

Figure 1.129: Histogram of the horizontally split events at 1487 eV

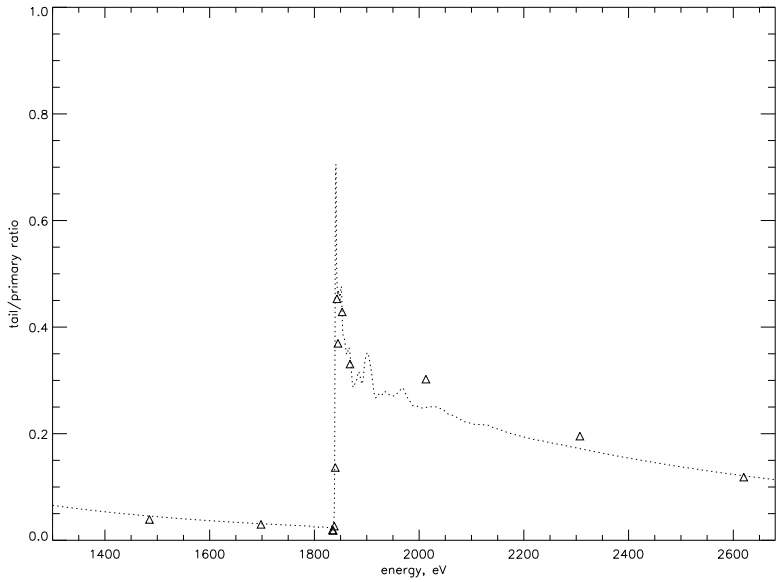

Figure 1.130: Ratio of the number of events in the shoulder to the total number of events in the horizontally split event histogram (triangles). Dotted line shows the calculated ratio assuming these events come from a layer of silicon 0.3 microns thick.

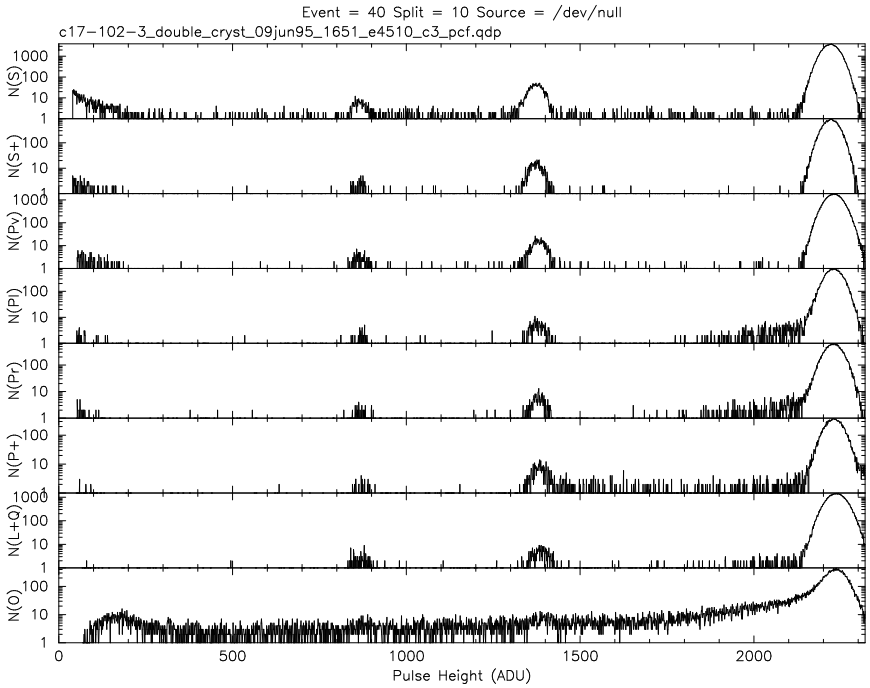

Figure 1.131: Standard graded histograms for experimental data taken with a monochromatic source at 4510 eV.

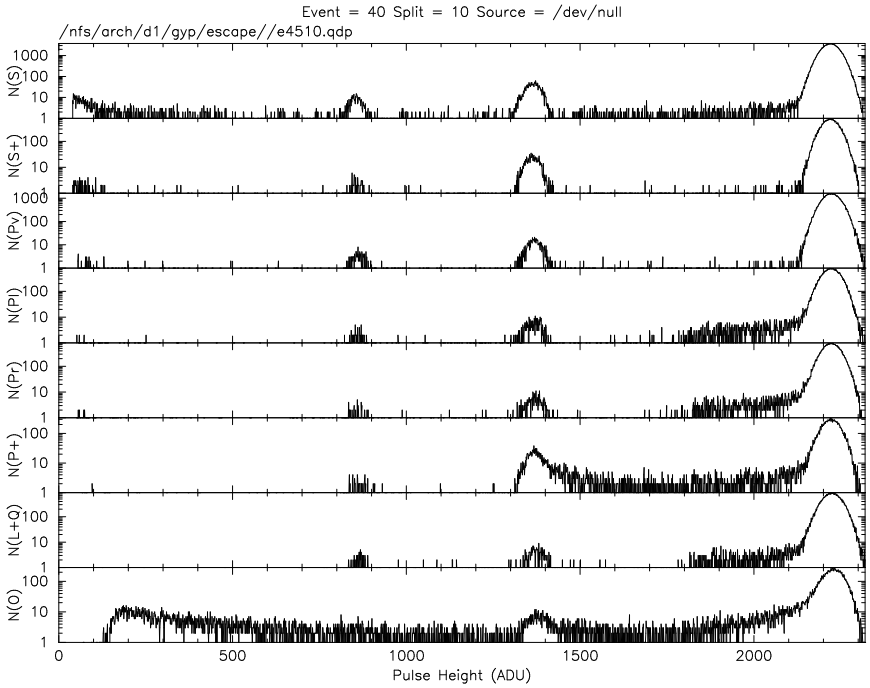

Figure 1.132: Standard graded histograms showing simulated response to 4510 eV X-rays.